Multi-turn, Tension-stiffening Catheter Navigation System

Yi Chen, Jean H. Chang, Alison S. Greenlee, Kenneth C. Cheung, Alex H. Slocum, and Rajiv Gupta

Abstract—In poorly constrained extra-vascular environments such as hollow viscera, current catheter navigation techniques are restricted to simple paths and therefore limit a doctor's ability to position the catheter. This paper presents a new catheter positioning system that enables faster and more accurate catheter placement, with fewer scans. The proposed robotic catheter navigation system can execute curved paths and maintain any number of three-dimensional turns using tension stiffening guide-wires composed of a set of disposable friction-locking beads. An external, reusable control system is used to automate the movement of the catheter. This control system uses a custom-designed graphical kinematic analysis program that predicts contact forces, changes in conformation due to external forces, tip deflection and failure modes of the catheter as it advances.

I. INTRODUCTION

DESPITE the widespread use of intra- and extra-vascular catheters and total catheter sales approaching an estimated $23 billion in 2009 [1], most catheters are rather simple devices consisting of a flexible plastic body and a maneuverable tip that is manipulated with pre-configured guide-wires. Catheters are therefore restricted to simple, primitive paths when guided through unconstrained areas. Present catheter positioning systems are especially limited in their accuracy and control when used for extra-vascular procedures – *e.g.*, the interventions performed in an unconstrained environment offered by a hollow viscera – because of the lack of external confinement provided by blood vessel walls. Under these circumstances, manual catheter positioning techniques that are currently in use sometimes require an extensive amount of time to position or reposition, resulting in increased risk to the collateral structures and unnecessary radiation exposure for the patient and the physician. These risks are being further exacerbated by the increasing complexity of newer procedures that may require penetration of several organ walls [2], the navigation along long curved paths, and the need to re-position in-dwelling catheters that have been left in place for several weeks [3].

The most common technique for positioning a catheter utilizes a guide wire with a pre-bent tip to steer the catheter to the desired location. Such systems restrict doctors to simple paths that cannot be altered once inside the patient. Several mechanical sheath-based [4] [5], push-twist controlled [6], or permanent magnet-based [7] [8] instruments are available. There are also multiple patents [9] [10] [11] that present the conceptual designs of devices being developed in industry. These products, such as the Venture^{TM} Wire Control Catheter [12] and the Artisan^{TM} Control Catheter [13], are only able to adjust the distal tip, use blood vessel walls to guide catheter shape, and do not allow the catheter to make multiple free-standing bends. In addition to these products, there are specialized medical robotic systems such as the HeartLander [14] that can only travel on a single continuous surface.

A system that would allow doctors to quickly and accurately maneuver a catheter in extra-vascular procedures is highly desirable. Examples of procedures that will benefit from such a device include any interventions inside hollow viscera such as the stomach or urinary bladder, navigation through solid organs, access for biopsy and drainage procedures, and intra-hepatic or trans-hepatic procedures such as portal vein access, biliary drainage and stone retrieval.

This paper describes a catheter positioning system that is able to maneuver a 9 French (3.0 mm diameter) catheter through extravascular spaces with an arbitrarily defined number of turns. Unlike other positioning systems, the proposed device is not bound to a set path and can readily make and maintain multiple turns at any time during the procedure. The system, named the Tension Stiffening Guide-wire (TSG), is composed of a low-cost, disposable section and a reusable control system. Using the control system, the doctor can intuitively control the position of the distal tip, the catheter advancement, and the curvature along the path of the catheter. Information from the control system can be used to indicate catheter position so that fewer fluoroscopic images are needed. The proposed system will hopefully reduce the time and the technical complexity of the existing procedure and will inspire the development of new minimally-invasive procedures that are currently performed though open surgery.

II. DESIGN

The functional requirements for the proposed catheter positioning system, which were developed after consultation with interventional radiologists and after observation of several procedures, are listed below.

1. Geometry: The device must be able to fit inside a 9 Fr catheter, and control a catheter up to 50 cm in length.

2. Navigation: The device must navigate catheters through unconstrained extravascular space, allow multiple user-directed turns, and be able to travel at speeds in excess of 1 cm/s.
3. Patient Motion: The device must be flexible enough so that patient movement will not result in injury. For example, the device should not be so rigid as to cause damage to the surrounding structures because of respiratory motion.
4. Scanning Compatibility: The system must be compatible with and visible under fluoroscopy, CT, and ultrasound imaging.
5. Safety: The system should not expose the patient to high voltages, electric current, hazardous substances, or high temperatures. In the event of an emergency, the device must be easily removable. Failure modes of the device must also be safe.
6. Cost: The portion of the device that enters the patient must be sterile, disposable and low-cost.
7. Control System: The device must be directly under a physician's control at all times.
8. User Interface: The device must be controllable in an intuitive way, in a manner similar to current catheter and guide-wire systems, to ease transition and decrease learning time.

Based on these requirements, many strategies were explored including pulling from the end effecter (suction, swimming, or biomechanical adhesives), externally driving (magnetic) and body shaping. For the given constraints, it was determined that a body shaping strategy would be the most suitable. The TSG catheter positioning system, conceptually shown in Figure 1, consists of two custom-designed "guide-wires" that can change their stiffness under user control. The two guide-wires used in this design are not identical. Guide-wire A has a body that can be stiffened and a distal end that can be maneuvered. Guide-wire B can only be stiffened or made flexible; it lacks the ability to maneuver the distal end. This double guide-wire positioning mechanism is placed inside the two central lumens of a multi-lumen sheath/catheter.

In operation, the guide-wires A and B are used in tandem: one guide-wire remains stiff while the other is kept flexible. The flexible guide wire uses the stiff guide wire as a reference "track" to move forward. The distal end of the flexible guide-wire A, which can be maneuvered to negotiate any arbitrary turn, is advanced under user control to "lengthen" the track. After the track has been advanced a suitable amount, the guide-wire A is stiffened while the guide-wire B is loosened. The catheter and the guide-wire B are advanced to the end of the newly developed track (i.e., tip of the guide-wire A). At this point the two guide-wires switch roles again and the guide-wire A lays down new track as before. Once this assembly reaches its final desired location, the two guide wires can be removed and the multi-lumen sheath/catheter left in place. Alternatively, the entire system can be exchanged for any other catheter using a conventional exchange guide-wire.
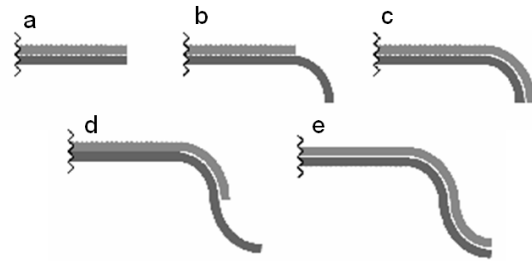

Fig. 1. Tandem-tracking method of alternating stiffness for catheter advancement. The catheter's initial configuration is shown in (a). In (b), the top guide-wire stiffness and is held rigid, while the lower guide-wire advances and deflects its tip. In (c), the lower guide-wire is held stiff, while the top guide-wire becomes flaccid and advances. This alternating progression continues in (d) and (e).

At first, the advancement of the system may seem difficult, analogous to pushing on a string. However, a more adequate analogy to the kinematics would be that of a train engine pushing a string of boxcars, which works just about as well as pulling boxcars. The tandem advancement of the system offers an advantage over other steerable multi-linked devices [15] as it does not compromise the shape of the previous path. Furthermore, the tip of the assembly has a firm base on which to deflect. The implementation of the disposable section can be separated into several functions: the controllable stiffness section, the deflectable tip, the coupling of the two guide-wires and the advancement strategy.

A. The Bead Strand Design

There are several ways to impart controllable stiffness to the main body of the guide-wires including the use of electrorheological or magnetorheological fluids. In the current design, a method using a strand of friction-locking beads was chosen. A tension wire (made of braided steel) runs through the strand of beads and allows the user to alter the load on the beads. The bulk lateral stiffness of the strand is proportional to the tension in the braided steel wire. Under tension, the shape of the strand of beads is maintained because the frictional force between the adjacent beads prohibits the beads from moving relative to each other.

A simple bead design was chosen for cost effectiveness and manufacturability. Beads with spherical bearing surface were designed to be stiffened by running a tension wire through the center. As shown in Figures 2a and 2b, the beads have toroidal holes, which prevent the wires from snagging and artificially straightening the strand. When the tension wire is loaded, the beads stack up against each other which causes friction (due to the roughness of the bearing surfaces) to lock the beads together. A set of beads with this particular geometry is able to maintain nearly any conformation when the tension wire is loaded. Once the tension in the wire is released, the beads unlock easily.
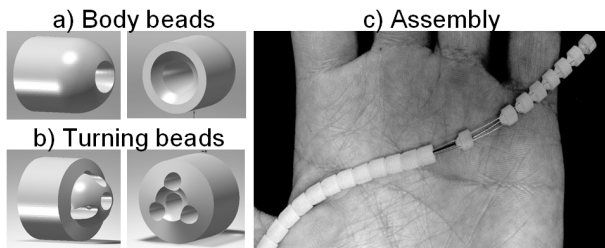
Fig. 2. Modular bead design and assembly prototyped via 3D printing. The body beads show in (a) are composed of spherical bearing surfaces to enable friction locking and a hole to allow control wires to pass through. The turning beads shown in (b) have multiple steering wire guides to enable the beads to tilt relative to each other. The steering guides run down the center of the body beads when the turning beads encounter the body beads. A large 6:1 mockup of the assembly is shown in (c).

B. Coupling and Advancement

Two strands are needed to maintain the catheter's configuration while it is advanced through body. One guide-wire (strand A) consists of body beads with a set of turning beads at the distal tip while the second guide-wire (strand B) only has body beads. A modular design consisting of two side-by-side strands inside an external encasement using a multi-lumen sheath was chosen to couple these two guide-wires. The multi-lumen sheath serves to maintain the separation between the two strands and prevent tissue entrapment between the beads. Figure 3 shows the custom-extruded cross-section. This design has the advantage of having safe failure modes; if the controlling wires break, the loose beads would be encased by the sheath and can be safely removed.

The multi-lumen sheath must be pliant enough to not compromise the shape of the controllable stiffness guide-wires, but stiff enough to avoid buckling around sharp turns. To minimize the abrasion between the sheath and the stiffening guide-wires, the material used for this application is Pebax with a durometer of 40D.
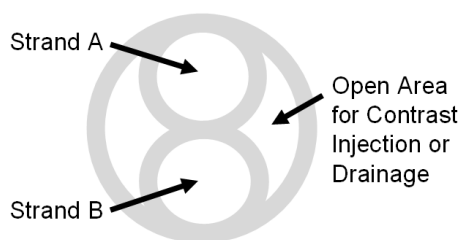

Fig. 3. Catheter sheath used to encase the two strands of controllable stiffness guide-wires. This design includes two unused lumens for contrast injection, drainage, or standard guide-wire insertion. These extra lumens also remove material from the sheath making it more flexible.

The concept behind the advancement strategy is based on a relative shifting and uncoiling technique. The catheter sheath and strands are stored in a helical coil form as in Figure 4. An advancement mechanism attached to strand B pushes forward to advance strand B with respect to strand A and pulls backward to advance strand A with respect to strand B while changing the coil conformation such that more of the TSG is advanced into the body.

C. Control System and Software

The complexity of advancement procedure, the precision required for the TSG movement, and the number of degrees of freedom require that the proposed catheter positioning system utilize a dedicated user-interface and control software. The control system operates six degrees of freedom and associated actuators: three for turning, two for locking and one for advancement (attached to the end of strand B). As shown in Figure 4, this permanent control system interfaces with the disposable catheter and TSG through a quick-connect plug.

The tension wires at the rear of the coiled TSG are attached to a series of force multiplying levers. These force levers decrease the step size and increase the force on the wires, resulting in relatively small and precise displacements. As a safety mechanism, the levers are programmed to never apply more force than the tension wires can tolerate.
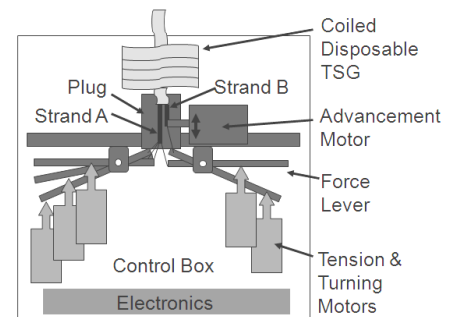

Fig. 4. Schematic of permanent control system. The schematic describes the location of the quick connect plug, the force levers, the motors, the electronics and the disposable TSG (including strand A and strand B).

In the current prototype, the force is provided by Haydon Switch and Instrument Series 20000 linear stepper motors. Linear steppers were chosen because of their ability to hold a position and move slowly and controllably. The linear steppers are driven by Gecko G251 stepper motor drivers. Other automation configurations were considered including linear Lorentz force coils and linear stages but stepper motors were considered easier to control.

A National Instruments USB-6501 data acquisition unit was used to interface the stepper drivers to a NI LabVIEW 8.5 program. A Logitech® Attack™ 3 joystick controls the tip deflection with respect to the locked body, while the buttons on the joystick control the advancement of the TSG. In the final version of the software, doctors will be able to image and establish the current location and configuration of the disposable TSG at any point in time. This information, along with the desired motion from the user interface, will be sent to a simulator which will display the simulated future position of the TSG. Once confirmed, the appropriate commands will be sent to the actuator motors. A schematic of software and hardware integration is shown in Figure 5.
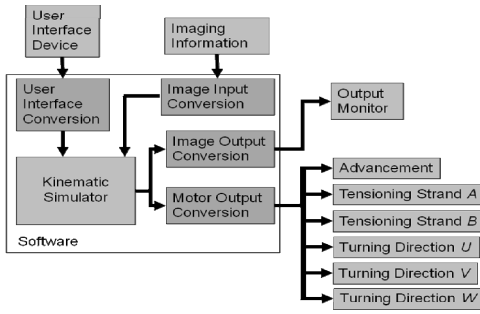
Fig. 5. Hardware and software integration. The user interface and the imaging system provide information to the kinematic simulator which projects the simulated motion of the TSG to a monitor and drives the motors.

III. KINEMATIC SIMULATION AND ANALYSIS

To predict the kinematics of the Tension Stiffening Guidewire, a software model was created in MATLAB. With this model, path planning, effects from changes in geometry, contact forces, change in conformation due to external forces, tip deflection, and failure modes can be predicted. The kinematic model consists of several modules which include: a three-dimensional graphing module, force and torque balance module, string reaction force module (using path minimization), and a tip deflection module. In the three-dimensional graphing module, a single bead is created by constructing line boundaries and utilizing a Cartesian coordinate location (x, y, z), and rotation (α, β) from the bead coordinate system to the absolute coordinate system. Figure 6 shows an assembled strand A.
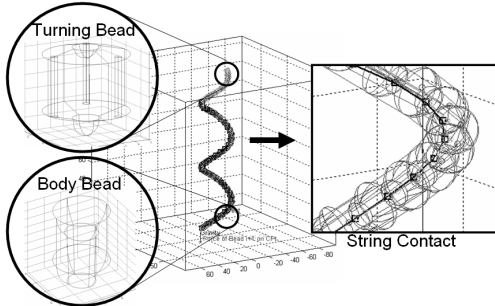

Fig. 6. Kinematic simulation of strand A. This simulation includes body beads, turning beads, force and torque balance as well as string contact. The string is visualized with the dark line and the contact points are visualized with squares.

The force module was created by taking into account external forces, tension reaction forces from internal strings, gravitational body forces, and acceleration forces from motion shown in Equation 1a. The forces are stored as $N \times 3$ (x, y, z) matrices while mass is stored as an $N \times 1$ vector and gravity and acceleration are stored as 1×3 vectors. Since the contact force on the top side of one bead is equivalent in magnitude to the contact force on the bottom of the next bead, all the contact forces at each bead surface can be solved at once using a finite difference matrix. Equation 1b shows the matrix that is used to solve for the forces in the x, y and z direction for all $N-1$ beads by matrix inversion.

$$\sum \vec{F} = \vec{F}^{ext} + \vec{F}^{t} + \vec{F}^{t2} + \vec{M} \times \vec{g} + \vec{M} \times \vec{a} \quad (1a)$$

$$\begin{bmatrix} -1 & 1 & \cdots & 0 \\ 0 & -1 & \ddots & 0 \\ \vdots & \vdots & \ddots & 1 \\ 0 & 0 & 0 & -1 \end{bmatrix} \begin{bmatrix} F_0{}^x & F_0{}^y & F_0{}^z \\ F_1{}^x & F_1{}^y & F_1{}^z \\ \vdots & \vdots & \vdots \\ F_N{}^x & F_N{}^y & F_N{}^z \end{bmatrix} = \sum \vec{F} \quad (1b)$$

The torque module solves for the unknown torques based on each of the previously balanced forces relative to the center of mass of each bead. The torque balance is accomplished using Equation 2 which is in vector form for each bead i including the following torques: external forces, forces from the bead above, forces from the bead below, and two contact forces for internal strings.

$$\sum T_i = \vec{L}_i^{ext} \times \vec{F}_i^{ext} + \vec{L}_i^a \times \vec{F}_i^a + \vec{L}_i^b \times \vec{F}_i^b + \vec{L}_i^t \times \vec{F}_i^t + \vec{L}_i^{t2} \times \vec{F}_i^{t2} \quad (2)$$

Using the known vector to the center of mass of each bead, length vectors are created using a transformation matrix for each of the corresponding forces. The cross product for each of these length and force vectors is combined and the resulting residual torque can then be compared with the normal forces on each surface. If the magnitude of the static frictional force is greater than the magnitude of the residual torque then the joint will hold, otherwise the joint will slip.

In order to find the string contact locations, a recursive maximum error elimination algorithm was created with the capability of determining if there was no contact point between a bead and the string and with the feature of being iteratively stable. The first step in the algorithm is to connect the start point at the first bead with the endpoint at the last bead with a vector. The next step is to search each bead in between to find the bead whose circular constraint (from the hole for the string) was furthest from the first vector. This is accomplished by finding a plane that describes the bottom and top holes of the bead. Since a plane can be defined by its normal and a constant, each level constant K_i in Equation 3a was found using the normal n_i. P_i is a point that falls within the circular constraint. After finding the definition of the plane, the intersection of the vector that connects the first bead and the last bead was found using Equation 3b.

$$K_i = \begin{bmatrix} x & y & z \end{bmatrix} \begin{bmatrix} n_x \\ n_y \\ n_z \end{bmatrix} = \vec{P}_i \bullet \vec{n}_i \quad (3a)$$

$$\vec{Q}_i = \vec{P}_{i-1} + \left[\frac{K_i - (\vec{P}_{i-1} \bullet \vec{n}_i)}{(\vec{P}_{i+1} - \vec{P}_i) \bullet \vec{n}_i} \right] \bullet (\vec{P}_{i+1} - \vec{P}_{i-1}) \quad (3b)$$

The output of this equation Q_i is a point on the vector between P_{i-1} and P_{i+1} that intersects a plane described by n_i and K_i. In the case of the first iteration, P_{i-1} would the contact point on the first bead and P_{i+1} would be the contact point on the last bead. This can then be used to construct the vector from the center of the hole to the Q_i which will intersect the contact point P_i on the circular constraint. If any contact point is in the wrong location due to the ordered nature of this process, this can be easily corrected by iteratively removing a random number of contact points and re-running the original algorithm. The algorithm stabilizes to the exact minimum path for a string in a constrained space. Figure 6 shows an example of the string contact.

From path minimization, reaction forces from string contact are calculated by finding the two vectors at each contact point and normalizing them. Then, the two vectors are added to produce the resultant string reaction force.

The tip deflection module predicts the location of the tip for a given initial condition and string tension sequence. When the string is first pulled, the turning bead nearest to the beginning will be the first to turn. When this bead comes into contact with another bead, the next gap begins to shorten. For a given length that a string is shortened, each gap decreases up to its maximum length which corresponds to a change in maximum angle. Partial shortening is scaled as a fraction of Equation 4.

$$\theta_{max} = 2\tan^{-1}((L_{center} - L_{outer})/D_{outer}) \quad (4)$$

L_{center} is the height of the material in the center of the turning bead, L_{outer} is the height of the bead at the location of the control string and D_{outer} is the diameter of the distance from the center of the bead to the location of the steering string hole. For three control strings separated by exactly 120°, the mapping for string contraction for each string to the coordinate system is:

Steering String U $\beta = \theta_u$

Steering String V $\alpha = (\sqrt{3}/2)\theta_v$ and $\beta = -(1/2)\theta_v$

Steering String W $\alpha = -(\sqrt{3}/2)\theta_w$ and $\beta = -(1/2)\theta_w$

Figure 7 shows how the tip changes when one of the strings is contracted incrementally. As more of the string is contracted, the tip turns more and more heavily. Using these modules in conjunction, controlling the catheter no longer needs to be completely closed loop. Rather, a closed loop control system can be supplemented with known deflections calculated with this model.
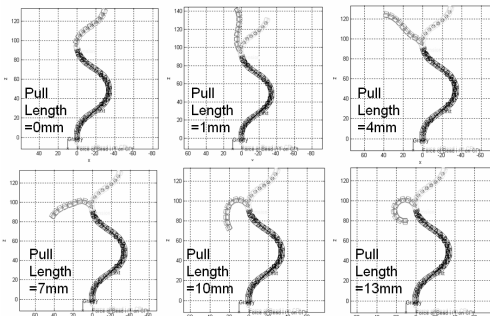

Fig. 7. Tip turning as the steering string is shortened from 0 to 13 mm for a scaled up 6:1 model of strand A.

IV. RESULTS

A. Scaling Forces and Dimensions

It is important to be able to develop simple scaling relationships that give insights to design. One important parameter to check is if the TSG will deform during patient motion (i.e. breathing). Estimates of the modulus of elasticity of internal organs vary substantially, but seem to converge on 20 kPa as a lower bound for organs such as the liver and spleen [16]. An adjacent organ can therefore provide up to 0.74 N of support for a 6 mm diameter by 6 mm long bead. This scaled up prototype made with plastic bearing surfaces has been shown experimentally to be able to resist transverse forces in the range of 0.18 N. Therefore, it will deform when it encounters an organ and will not puncture the organ under normal circumstances. The relationship between the organ support force and the transverse resistance force will scale down to 1 mm by 1 mm beads and further testing will be needed to determine the holding forces for sub-millimeter beads.

The maximum length of TSG that is able to resist torques applied to the end was also investigated. The breaking strength of the cable is defined as F_{max}, the force applied to the tip is defined as F_t and the length of the TSG is defined as L. By balancing the torques, the maximum length of TSG that can resist a disturbance at the tip without deforming can be found from $F_t L < \mu_s l F_{max}$, where l is the distance from the holding position to the nearest friction interface and μ_s is the static coefficient of friction between beads. For a reasonable coefficient of friction of 0.6, a bead length of 6 mm, F_{max} of 30 N (experimentally determined for PTFE coated steel cable with a diameter of 0.35 mm), and a tip force of 0.2 N, the upper bound to the maximum length of the TSG is 54 cm, which meets the specifications. Since some deformation is allowed for patient motion, stronger cable like Aramid (F_{max}=348 N) can be used for the 1 mm beads and the length of the conformable section will generally be less than 50 cm, this relationship shows that the TSG concept will not only work but can also be built from conventional materials.

Another important question is maneuverability, which can be determined by looking at the bead to bead interface friction as well as the friction from the string to the bead. At any given bead to bead interface, the force of static friction must be greater than the force generated by the string against the interface such that $\mu_s F_s > 2F_s cos(\varphi)$ where φ is the half angle between the beads and F_s is the tension force. Therefore, a higher static coefficient of friction at the bead to bead interface will give a tighter turning radius. From the point of view of the friction between a string and a bead, the number of turns in the system will affect the ability to both pull cables and push the advancing TSG forward. If the TSG is straight, F_t at the control end of the TSG is required. With multiple turns, an upper bound on the normal force F_{ni} of twice the tension force (as if the system is acting as a mechanical pulley with a 180° turn) is needed to reach the previous turn, F_{ni-1}, with enough force to achieve F_t at the tip. Therefore, the necessary maximum coefficient of friction between the string and bead μ_f given M number of turns, is given in Equation 5a, where the normal force utilized for each calculation must cascade down from turn to turn reducing to equation 5b.

$$F_{max} = F_t + \mu_f \sum_{i=1}^{M} F_{ni} = F_t(1 + 2\mu_f + 2\mu_f(1 + 2\mu_f) + ...) \quad (5a)$$

$$F_{max} = F_t(1 + 2\mu_f)^M \quad (5b)$$

Using F_{max} of 30 N and F_t of 5 N (cable pulling force necessary to overcome a 1 N snag force), as well as a μ_f of 0.04 (lubricated PTFE bearings), this predicts an upper bound of fifteen 180° turns before operational forces would exceed the breaking strength of the control cables. Given these results, the torque resistance limit will be reached before the maneuverability limit of the strings is reached.

This result also predicts that the maximum string tension, and thereby the overall maneuverability, of this type system can be improved linearly with increasing tensile strength of the actuation cables and improved to the power M by decreasing μ_f.

B. Scanning

The TSG assembly must be compatible and detectable with multiple scanning methods. Figure 8 shows the 3D reconstructions and CT scans completed at the Radiology Department at Massachusetts General Hospital on a Siemens Somatom Sensation 64 machine. Although the beads are made of plastics and are relatively invisible while in the body, the control and tensioning wires made of steel show up fairly strongly on scans. In addition, steel inserts at the end of the turning beads shown in Figure 8c allow the imaging device to find the tip of the TSG and will allow the kinematic simulator to determine the orientation of the tip.
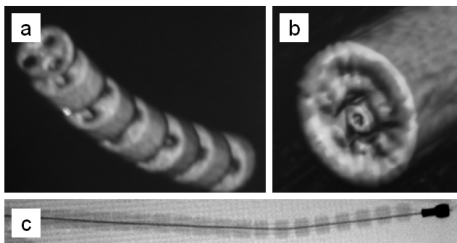

Fig. 8. CT images of device. Panel (a) shows a 3d reconstruction of an individual strand while (b) shows a 3d reconstruction of an encapsulated strand. Panel (c) shows a fluoroscopy image of strand A along with body beads, turning beads and control wires.

V. Conclusions and Future Work

The catheter positioning system is a novel device that can accurately maneuver and position catheters in both intra- and extra-vascular procedures. It allows for more advanced procedures, shorter procedure times and a reduction in the number of scans needed. This concept, which is protected by a provisional patent, has the potential for many non-medical applications including the navigation of a 'snakebot' through small openings.

Further development is needed to advance this catheter positioning system to an off-the-shelf medical tool. First, the TSGs will be scaled down using more advanced manufacturing techniques. The material and surface finish of the beads will need to be carefully chosen so that there is enough friction between the beads when they are fabricated by mass production methods. Possible methods for producing the desired surface roughness include sand-blasting and powder coating. A custom-extruded multi-lumen encasement catheter of appropriate size will also need to be fabricated. A more compact control system with more powerful actuators is needed to increase the navigational speed. For the custom user interface, additional upgrades to the software are also necessary, including interfacing with the imaging information and output monitor. We have completed a first order validation of the model; future work includes a more extensive validation of the kinematic model under various realistic conditions. Finally, applications for this positioning system must be expanded to other procedures by integration with different types of catheters.

References

[1] B. Breindel, "The catheter business: How much? Who? Where?" BCC Research, Wellesley, MA, HLC019B, 2004.

[2] J. T. Ferrucci, P. R. Mueller, and W. P. Harbin, "Percutaneous transhepatic biliary drainage," *Diagnostic Radiology*, vol. 135, pp. 1-13, 1980.

[3] K. Mori, A. Misumi, M. Sugiyama, M. Okabe, T. Matsuoka, J. Ishii, and M. Akagi, "Percutaneous transhepatic bile drainage," *Annuals of Surgery*, vol. 185, no. 1, pp. 111-115, 1977.

[4] V. Y. Reddy, P. Neuzil, Z. J. Malchano, R. Vijaykumar, R. Cury, S. Abbara, J. Weichet, C. D. McPherson, and J. N. Ruskin, "View-synchronized robotic image-guided therapy for atrial fibrillation ablation: Experimental validation and clinical feasibility," *Circulation*, vol. 115, pp. 2705-2714, 2007.

[5] N. Simaan, R. Taylor, A. Hillel, and P. Flint, "Minimally invasive surgery of the upper airways: Addressing the challenges of dexterity enhancement in confined spaces," *Surgical Robotics: History, Present and Future Applications*, R. A. Faust, Ed. New York: Nova Science Publishers, 2006, pp. 261-280.

[6] Y. Thakur, C. J. Norley, D. W. Holdsworth, and M. Dragova, "Remote v. manual catheter navigation: A comparison study of operator performance using a 2D multi-path phantom," *Proceedings of SPIE Medical Imaging 2009: Visualization, Image-Guided Procedures, and Modeling*, vol. 7261, pp. 1A1-1A7, 2009.

[7] M. Schiemann, R. Killmann, M. Kleen, N. Abolmaali, J. Finney, and T. J. Vogl, "Vascular guide wire navigation with a magnetic guidance system: Experimental results in a phantom," *Radiology*, vol. 232, pp. 475-481, 2004.

[8] M. N. Faddis, W. Blume, J. Finney, A. Hall, J. Rauch, J. Sell, K. T. Bae, M. Talcott, and B. Lindsay, "Novel, magnetically guided catheter for endocardial mapping and radiofrequency catheter ablation," *Circulation*, vol. 106, pp. 2980-2985, 2002.

[9] M. A. Martinelli and W. C. Haase, "Method and system for navigating a catheter probe," U. S. Patent RE40,852, July 14, 2009.

[10] M. Eng, R. R. Viswanathan, P. R. Werp, I. Tunay, A. K. Pandey, and G. T. Munger, "Electrophysiology catheter," U. S. Patent 6,980,843, Dec. 27, 2005.

[11] R. I. Rudko, C. C. Negus, S. J. Linhares and E. A. Woodruff, "Catheter navigation apparatus," U. S. Patent 5,830,210, Nov. 3, 1998.

[12] P. O'Kane, L. Blows, and S. Redwood, "The Venture™ Wire Control Catheter," *The British Journal of Cardiology*, vol. 14, Issue 5, pp. 293-295, 2007.

[13] P. Kanagaratnam, M. Koa-Wing, D. T. Wallace, A. S. Goldenberg, N. S. Peters, and D. W. Davies, "Experience of robotic catheter ablation in humans using a novel remotely steerable catheter sheath," *Journal of Interventional Cardiac Electrophysiology*, vol. 21, pp. 19-26, 2008.

[14] N. Patronik, M. A. Zenati, and C. Riviere, "Preliminary evaluation of a mobile robotic device for navigation and intervention on the beating heart," *Computer Aided Surgery*, vol. 10, no. 4, pp. 225-232, 2005.

[15] B. Zubiate, H. M. Choset, A. Degani, M. Schwerin, "Steerable multi-linked device having a modular link assembly," U. S. Patent 2008163603, July 10, 2008.

[16] J. Stingl, V. Báĉa, P. Ĉech, J. Kovanda, H. Kovandová, V. Mandys, J. Rejmontová, and B. Sosna, "Morphology and some biomechanical properties of human liver and spleen," *Surgical and Radiologic Anatomy*, vol. 24, pp. 285–289, 2002.